



## **CD40 Agonists Alter Tumor Stroma and Show Efficacy Against Pancreatic Carcinoma in Mice and Humans**

Gregory L. Beatty, et al. Science **331**, 1612 (2011); DOI: 10.1126/science.1198443

This copy is for your personal, non-commercial use only.

If you wish to distribute this article to others, you can order high-quality copies for your colleagues, clients, or customers by clicking here.

**Permission to republish or repurpose articles or portions of articles** can be obtained by following the guidelines here.

The following resources related to this article are available online at www.sciencemag.org (this infomation is current as of March 24, 2011):

**Updated information and services,** including high-resolution figures, can be found in the online version of this article at:

http://www.sciencemag.org/content/331/6024/1612.full.html

Supporting Online Material can be found at:

http://www.sciencemag.org/content/suppl/2011/03/22/331.6024.1612.DC1.html

This article **cites 22 articles**, 8 of which can be accessed free: http://www.sciencemag.org/content/331/6024/1612.full.html#ref-list-1

This article appears in the following **subject collections**: Medicine, Diseases

http://www.sciencemag.org/cgi/collection/medicine

ecosystem structure. Our study shows that declines in salmon will have the largest ecological impacts on smaller and less productive streams. In contrast, large and shallow-sloped watersheds dominated by nitrogen-fixing red alders are predicted to be more resilient to salmon declines. These considerations enable predictions of impacts of anthropogenic stressors across ecosystem boundaries, which can then be incorporated into ecosystem-based management.

### References and Notes

- 1. B. Worm et al., Science 314, 787 (2006).
- 2. J. B. C. Jackson et al., Science 293, 629 (2001).
- 3. H. K. Lotze et al., Science 312, 1806 (2006).
- 4. G. A. Polis, S. D. Hurd, Am. Nat. 147, 396 (1996).
- D. A. Croll, J. L. Maron, J. A. Estes, E. M. Danner, G. V. Byrd, Science 307, 1959 (2005).
- 6. J. L. Maron et al., Ecol. Monogr. 76, 3 (2006).
- L. B. Marczak, R. M. Thompson, J. S. Richardson, *Ecology* 88, 140 (2007).
- S. M. Gende, R. T. Edwards, M. F. Willson, M. S. Wipfli, Bioscience 52, 917 (2002).
- R. J. Naiman, R. E. Bilby, D. E. Schindler, J. M. Helfield, *Ecosystems* 5, 399 (2002).
- D. J. Janetski, D. T. Chaloner, S. D. Tiegs, G. A. Lamberti, *Oecologia* 159, 583 (2009).
- J. W. Moore, D. E. Schindler, Can. J. Fish. Aquat. Sci. 61, 1582 (2004).
- 12. J. W. Moore et al., Ecology 88, 1278 (2007).
- 13. S. D. Tiegs et al., Ecol. Appl. 18, 4 (2008).

- 14. J. M. Helfield, R. J. Naiman, Oecologia 133, 573 (2002).
- 15. See supporting material on Science Online.
- M. H. H. Price, C. T. Darimont, N. F. Temple,
  M. MacDuffee, Can. J. Fish. Aquat. Sci. 65, 2712 (2008).
- 17. T. E. Reimchen, Can. J. Zool. 78, 448 (2000).
- 18. C. T. Darimont, P. C. Paquet, T. E. Reimchen, *BMC Ecol.* **8.** 14 (2008).
- 19. R. E. Bilby, B. R. Fransen, P. A. Bisson, *Can. J. Fish. Aquat. Sci.* **53**, 164 (1996).
- 20. K. K. Bartz, R. J. Naiman, Ecosystems 8, 529 (2005).
- C. E. Wilkinson, M. D. Hocking, T. E. Reimchen, *Oikos* 108, 85 (2005).
- M. D. Hocking, T. E. Reimchen, *Oikos* 118, 1307 (2009).
- K. Klinka, V. J. Krajina, A. Ceska, A. M. Scagel, *Indicator Plants of Coastal British Columbia* (Univ. of British Columbia Press, Vancouver, 1989).
- 24. J. M. Diez, H. R. Pulliam, Ecology 88, 3144 (2007).
- A. F. Zuur, E. N. Ieno, N. J. Walker, A. A. Saveliev, G. M. Smith, Mixed Effects Models and Extensions in Ecology with R (Springer Science+Business Media, New York, 2009).
- 26. P. A. Alaback, Ecology 63, 1932 (1982).
- J. Pojar, K. Klinka, D. V. Meidinger, For. Ecol. Manage. 22, 119 (1987).
- 28. G. Pinay, T. O'Keefe, R. Edwards, R. J. Naiman, *Ecosystems* **6**, 336 (2003).
- 29. E. A. Hobbie, J. E. Hobbie, Ecosystems 11, 815 (2008).
- 30. J. M. Craine et al., New Phytol. 183, 980 (2009).
- J. M. Kranabetter, W. H. MacKenzie, *Ecosystems* 13, 108 (2010).
- J. J. Verspoor, D. C. Braun, J. D. Reynolds, *Ecosystems* 13, 1020 (2010).

- R. E. Bilby, B. R. Fransen, J. K. Walter, C. J. Cederholm, W. J. Scarlett, Fisheries 26, 6 (2001).
- 34. DFO (Fisheries and Oceans Canada, Vancouver, 2005).
- 35. C. T. Darimont et al., Conserv. Lett. 3, 379 (2010).
- 36. D. E. Schindler et al., Nature 465, 609 (2010).
- 37. Supported by the Tom Buell Endowment Fund at Simon Fraser University (SFU), a Natural Science and Engineering Research Council of Canada (NSERC) postdoctoral fellowship (M.D.H.), NSERC Discovery and Accelerator grants (J.D.R.), the B.C. Leading Edge Endowment Fund, the Pacific Salmon Foundation, the B.C. Pacific Salmon Forum, and Mountain Equipment Co-op. We thank C. Aries for plant surveys; D. Braun, A. Cooper, E. Darling, N. Dulvy, R. Field, J. Harding, J. Linton, M. Stubbs, W. Palen, J. Verspoor, and the Earth<sub>2</sub>Ocean Research Group at SFU for discussions and analytical support; A. Albright, J. Barlow, J. Beaudin, J. Gordon-Walker, I. Jansma, E. Nelson, M. Spoljaric, 1 Wilson, and the Raincoast Conservation Foundation for field support; R. Carpenter, M. Reid, and others at the Heiltsuk Integrated Resource Management Department; L. Jorgenson from Qqs Projects Society in Bella Bella; and the Heiltsuk Nation for research partnerships in their traditional territory.

## Supporting Online Material

www.sciencemag.org/cgi/content/full/331/6024/1609/DC1 Materials and Methods

SOM Text Figs. S1 to S5 Tables S1 to S13 References

30 November 2010; accepted 25 January 2011 10.1126/science.1201079

# CD40 Agonists Alter Tumor Stroma and Show Efficacy Against Pancreatic Carcinoma in Mice and Humans

Gregory L. Beatty, <sup>1,2,6</sup> Elena G. Chiorean, <sup>3</sup> Matthew P. Fishman, <sup>1</sup> Babak Saboury, <sup>5</sup> Ursina R. Teitelbaum, <sup>2,6</sup> Weijing Sun, <sup>2,6</sup> Richard D. Huhn, <sup>4</sup> Wenru Song, <sup>4</sup> Dongguang Li, <sup>4</sup> Leslie L. Sharp, <sup>4</sup> Drew A. Torigian, <sup>2,5</sup> Peter J. O'Dwyer, <sup>2,6</sup> Robert H. Vonderheide <sup>1,2,6</sup>\*

Immunosuppressive tumor microenvironments can restrain antitumor immunity, particularly in pancreatic ductal adenocarcinoma (PDA). Because CD40 activation can reverse immune suppression and drive antitumor T cell responses, we tested the combination of an agonist CD40 antibody with gemcitabine chemotherapy in a small cohort of patients with surgically incurable PDA and observed tumor regressions in some patients. We reproduced this treatment effect in a genetically engineered mouse model of PDA and found unexpectedly that tumor regression required macrophages but not T cells or gemcitabine. CD40-activated macrophages rapidly infiltrated tumors, became tumoricidal, and facilitated the depletion of tumor stroma. Thus, cancer immune surveillance does not necessarily depend on therapy-induced T cells; rather, our findings demonstrate a CD40-dependent mechanism for targeting tumor stroma in the treatment of cancer.

Pancreatic ductal adenocarcinoma (PDA) remains an almost universally lethal disease; chemotherapy offers minimal benefit over best supportive care for patients who are not surgical candidates (1). We have previously demonstrated that leukocytes actively infiltrate the stromal compartment of PDA, even at the earliest stages of tumor development, and orchestrate an immune reaction that is immunosuppressive (2). In this study, we investigated the reversibility of this immune suppression, hy-

pothesizing initially that doing so would unleash tumor-specific cellular immunity to eliminate PDA. Activation of the tumor necrosis factor (TNF) receptor superfamily member CD40 has been shown to be a key regulatory step in the development of T cell–dependent antitumor immunity, which relies on CD40-mediated "licensing" of antigen-presenting cells (APCs) for tumor-specific T cell priming and activation (3–8).

On the basis of this premise, we investigated in both humans and mice whether systemic CD40 activation with an agonist CD40 monoclonal antibody (mAb) can circumvent tumor-induced immune suppression and invoke productive T cell-dependent antitumor immunity in PDA. We first evaluated the clinical impact of CD40 activation by performing a clinical trial of the fully human agonist CD40 mAb CP-870,893 (9) in combination with gemcitabine chemotherapy (2'-deoxy-2',2'-difluorocytidine) for patients with chemotherapy-naïve, surgically incurable PDA (10). We tested CP-870,893 with gemcitabine because chemotherapy delivered before an agonist CD40 mAb can facilitate enhanced tumor antigen presentation by APCs (11–14). Twenty-one patients (90% with metastatic disease) received gemcitabine weekly on days 1, 8, and 15 with CP-870,893 administered on day 3 of each 28day cycle (fig. S1). Treatment was well tolerated overall (fig. S2), and the most common side effect was mild-to-moderate cytokine release syndrome characterized by chills, fevers, rigors, and other symptoms on the day of CP-870,893

<sup>1</sup>Abramson Family Cancer Research Institute, University of Pennsylvania School of Medicine, 421 Curie Boulevard, Philadelphia, PA 19104, USA. <sup>2</sup>Abramson Cancer Center, University of Pennsylvania School of Medicine, Philadelphia, PA 19104, USA. <sup>3</sup>Division of Hematology/Oncology, Department of Medicine, Indiana University School of Medicine, Indianapolis, IN 46202, USA. <sup>4</sup>Pfizer Corporation, New London, CT 06320, USA. <sup>5</sup>Department of Radiology, Department of Medicine, University of Pennsylvania School of Medicine, Philadelphia, PA 19104, USA. <sup>6</sup>Division of Hematology-Oncology, Department of Medicine, University of Pennsylvania School of Medicine, Philadelphia, PA 19104, USA.

\*To whom correspondence should be addressed. E-mail: rhv@exchange.upenn.edu

infusion. Symptoms were transient (<24 hours) and managed in the outpatient clinic with supportive care.

The impact of therapy on the primary and metastatic lesions was evaluated using two standard modalities: (i) [18F]2-fluoro-2-deoxy-D-glucose (FDG) avidity on positron emission tomography-computed tomography (PET-CT) as a measure of an on-target biological effect of therapy and (ii) CT imaging for Response Evaluation Criteria in Solid Tumors (RECIST) assessment. Metabolic responses were observed by FDG-PET-CT in both the primary and metastatic lesions in 88% of patients evaluated after two cycles of therapy (fig. S3). By RECIST, 4 out of 21 patients developed a partial response (PR), 11 patients had stable disease (SD), and 4 patients had progressive disease (PD) (Fig. 1A). Two patients were not evaluable on study for tumor response. One of these patients (patient 10031010) was taken off the study protocol after one dose of CP-870,893 because of a grade 4 cerebrovascular accident but recovered neurologically and restarted gemcitabine alone and achieved a PR. The second patient (patient 10031001) had clinical deterioration from disease progression, and posttherapy CT imaging was not obtained. The median progression-free survival (PFS) for the 21 patients was 5.6 months (95% confidence interval, 4.0 months to not estimable), and the median overall survival (OS) was 7.4 months (95% confidence interval, 5.5 to 12.8 months). Median PFS and OS are based

on interim data as of 25 August 2010, with 6 of 21 patients alive. Gemcitabine alone achieves a historical tumor response rate of 5.4%, with median PFS of 2.3 months and median OS of 5.7 months (1). Therefore, treatment with CP-870,893 and gemcitabine showed therapeutic efficacy in patients with metastatic PDA.

One patient with a PR showed a 46% reduction in the primary pancreatic lesion, complete resolution of a 7.6-cm hepatic metastasis, and 47% reduction in the one remaining hepatic metastasis (Fig. 1B). Upon biopsy after four cycles of therapy, this remaining liver lesion showed no viable tumor. Instead, we observed necrosis and an infiltrate dominated by macrophages with an absence of lymphocytes (Fig. 1C). A second patient with a PR underwent surgical resection of the primary tumor after achieving a complete resolution of all hepatic metastases and a 64% reduction in the primary pancreatic lesion. Histological analysis of the resected primary lesion revealed a cellular infiltrate devoid of lymphocytes (Fig. 1C). Such tumor regression without lymphocyte infiltration was unexpected on the basis of results from implantable tumor models, where CD40-induced antitumor activity is dependent on T cells (6-8). Therefore, to understand the mechanism of CD40mediated tumor regression, we turned to a spontaneous mouse model of PDA.

The KPC model of PDA is a genetically engineered mouse model that incorporates the conditional expression of both mutant Kras G12D

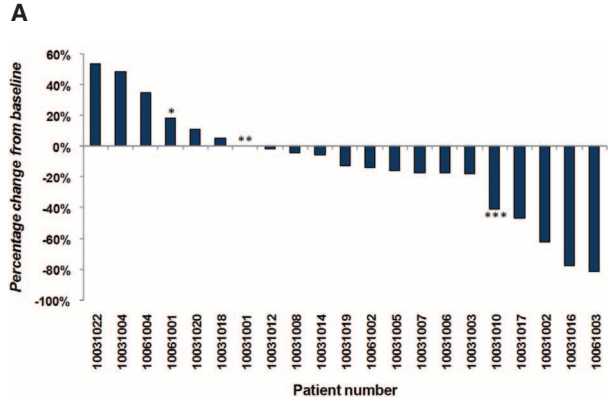
В

10031016

and  $p53^{R172H}$  alleles in pancreatic cells (15). Because immunocompetent KPC mice spontaneously develop PDA tumors that display high fidelity to the histopathologic and molecular features of human PDA (15), the KPC model is thought to be relevant for understanding treatment mechanisms in patients (16, 17). We therefore modeled our clinical study in KPC mice by evaluating the therapeutic efficacy of gemcitabine weekly with the agonist CD40 mAb FGK45 administered 48 hours after the first infusion of gemcitabine. Tumor response was monitored by three-dimensional ultrasonography (fig. S4) (10). We found that the combination of FGK45 with gemcitabine induced tumor regression in 30% of mice (Fig. 2A), similar to the objective response rate in our patients. Treatment with FGK45 alone resulted in the same rate of tumor regression, whereas gemcitabine alone did not (Fig. 2A).

Activation of the CD40 pathway is a critical event in the development of tumor-specific T cell immunity (18). To test whether CD40 immunotherapy is dependent on T cell activation, we examined the function of T cells isolated from the spleen and pancreas (including tumor and peripancreatic lymph nodes) of KPC mice. Seven days after treatment with FGK45, both CD4<sup>+</sup> and CD8<sup>+</sup> T cells of KPC mice acquired an increased capacity to secrete cytokines, including interferon-y (IFN-y) and interleukin IL-17A (fig. S5A); however, FGK45 induced the same rate of tumor regression in KPC mice in the absence of CD4<sup>+</sup> or CD8<sup>+</sup> cells or both CD4<sup>+</sup>

10031016 Liver Metastasis



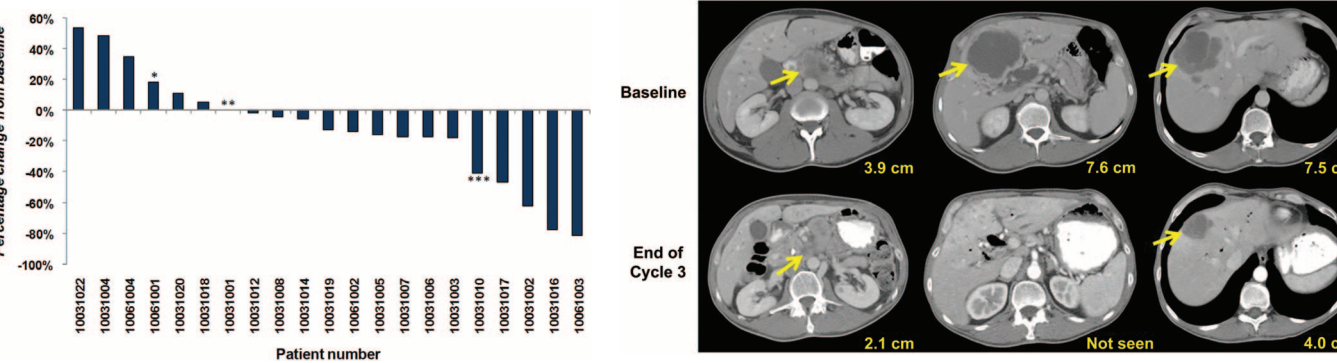


Fig. 1. Agonist CD40 mAb in combination with gemcitabine induces clinical responses in patients with surgically incurable PDA. (A) Best overall percentage of change from baseline in tumor target lesion measurement shown as a waterfall plot. \*Patient 10061001 was defined as PD because of the appearance of a new nontarget lesion. \*\*Patient 10031001 did not obtain posttherapy scans because of clinical deterioration from disease progression after one dose of CP-870,893. \*\*\*Patient 10031010 came off the study after one dose of CP-870,893 but restarted gemcitabine alone and achieved a PR. (B) CT imaging obtained at baseline and end of cycle 3. The primary pancreatic tumor and two metastatic liver lesions are marked by arrows, with the longest dimension annotated. (C) Histopathology of a biopsied metastatic lesion [from patient 10031016 (left)] and a surgically resected primary pancreatic

10031016 10061003 **Liver Metastasis Primary Tumo**i

10031016 Liver Metastasis

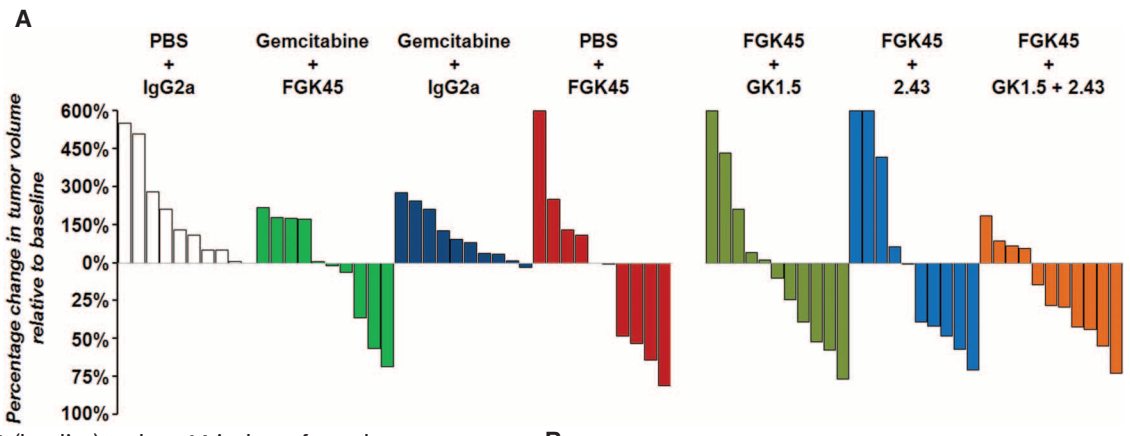
lesion [from patient 10061003 (right)]. Both patients achieved a PR. Patient 10031016 underwent tumor biopsy after completing four cycles of therapy; patient 10061003 underwent surgical resection of the primary tumor after 12 cycles of therapy. Arrows (left) indicate a macrophage-dominated inflammatory infiltrate within extensive tumor necrosis. Arrows (right) identify polymorphonuclear infiltrating cells without lymphocytes; arrowheads mark tumor cells. Scale bars, 50 µm.

and CD8<sup>+</sup> cells (Fig. 2A). This was unexpected given the established link between CD40 activation and the development of productive antitumor T cell immunity (6–8). Histopathological appearance of tumors from responder compared with nonresponder animals at day 14 was sim-

ilar overall, with the exception that tumors were smaller in responder animals (Fig. 2, B to E). CD3<sup>+</sup> T cells were not observed to infiltrate tumors in KPC mice at baseline or at any time after treatment with FGK45 (Fig. 2, F to H). Instead, CD3<sup>+</sup> T cells remained localized to

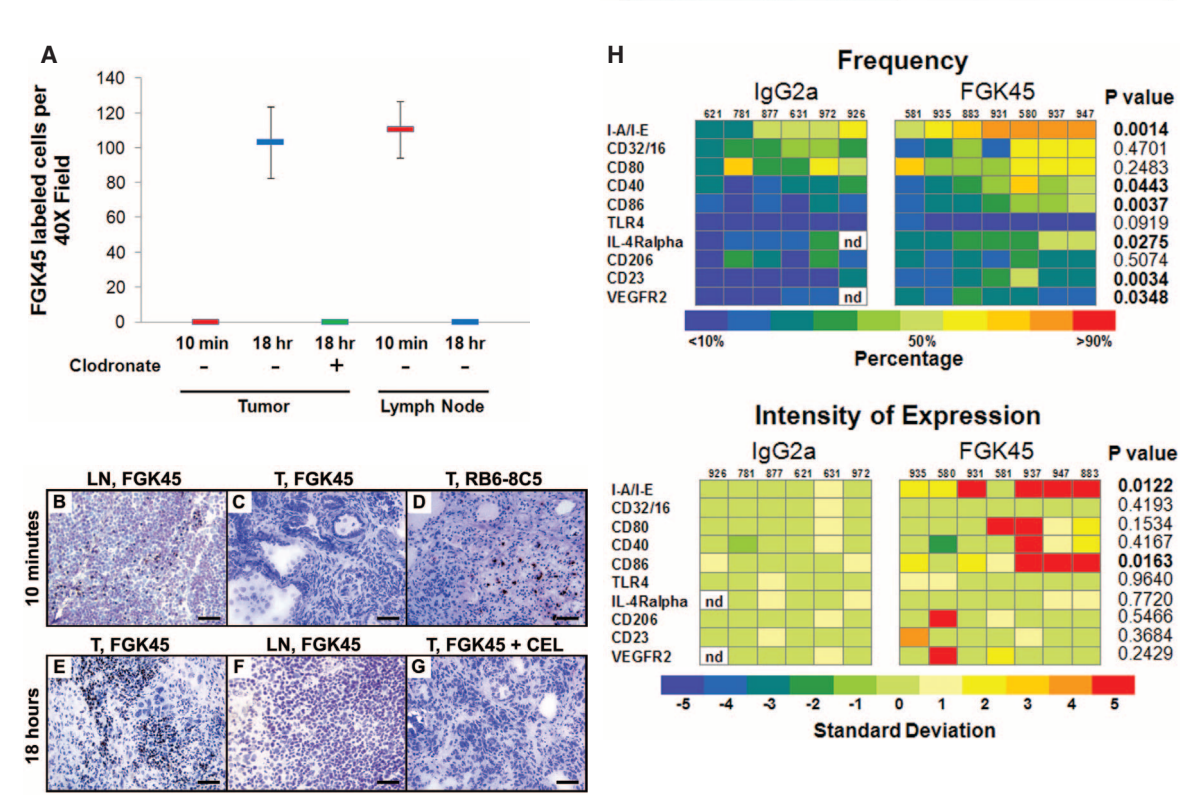
peripancreatic lymph nodes situated adjacent to developing tumors (Fig. 2, E and I). Moreover, when the whole pancreas was resected en bloc with peripancreatic lymph nodes, CD3<sup>+</sup> T cells did not change in frequency before and after therapy (fig. S5, B and C). Thus, activation of

Fig. 2. Antitumor activity of agonist CD40 mAb in KPC mice is T cell-independent. (A) KPC mice were treated with gemcitabine or phosphatebuffered saline (PBS) on day 0 and day 7, with control IgG2a or FGK45 administered on day 2. Cohorts of KPC mice receiving treatment with FGK45 were also depleted of CD4+ or CD8+ cells or both CD4+ and CD8<sup>+</sup> cells with the use of GK1.5 and 2.43 antibodies, respectively, on days -1, 0, 1, 3, 7, and 10. Percent change



in tumor volume from day -1 (baseline) to day +14 is shown for each mouse as a waterfall plot (in comparison with PBS + IgG2a, gemcitabine + FGK45: P < 0.05; gemcitabine + IgG2a: P = 1.00; PBS + FGK45: P < 0.05; FGK45 + GK1.5: P < 0.05; FGK45 + GK1.5: P < 0.05; FGK45 + GK1.5: P < 0.05; Fisher's exact test). Hematoxylin and eosin (H&E) histology [(B) to (E)] and CD3 immunohistochemistry [(F) to (I)] are shown for tumors from KPC mice treated with IgG2a (**B** and **F**) or FGK45 (**C** to **E** and **G** to **I**). Responders (D), (E), (H), and (I) were defined as FGK45-treated mice that demonstrated tumor regression by ultrasound analysis. FGK45-treated mice with tumor progression by ultrasound were defined as nonresponders (C) and (G). Scale bars, 50  $\mu$ m.

Fig. 3. Agonist CD40 mAb targets systemic macrophages before their infiltration of tumor. Immunohistochemistry was used to quantify leukocyte infiltration (A) into peripancreatic lymph nodes (A, B, and F) and KPC tumor (A, C, D, E, and G) by staining with a biotinylated goat antibody directed against rat IgG to detect FGK45 or RB6-8C5 bound to cells at 10 min (A) to (D) or 18 hours (A) and (E) to (G) after treatment. Macrophages were depleted with CELs before FGK45 treatment (A) and (G). LN, peripancreatic lymph node; T, tumor; scale bars, 50 μm. Error bars in (A) represent SD. (H) A heat map displaying the flow cytometric analysis of tumorassociated macrophages from individual KPC mice (columns) for expression



of cell surface molecules (rows) 3 days after treatment with control IgG2a compared with FGK45. (Top) The percentage of tumor-associated macrophages with surface molecule expression. (Bottom) Mean fluorescence intensity as the

number of standard deviations from the mean, which was determined from treatment with control IgG2a. P values are based on Student's t test; nd, not determined.

Tumor +

KPC Mø (FGK45)

the CD40 pathway does not trigger T cell infiltration into tumors and is insufficient to induce productive antitumor T cell immunity in the KPC model.

CD40 is expressed on a wide range of leukocytes including monocytes, tissue macrophages, B cells, and dendritic cells and can also be found on some tumors (19). By immunohistochemistry, we found that PDA cells were CD40-negative, whereas cells in the tumor stroma expressed CD40, particularly F4/80<sup>+</sup> tumorassociated macrophages (fig. S6). We therefore investigated the impact of CD40 immunotherapy on F4/80<sup>+</sup> macrophages in KPC mice. Within 18 hours of administration, FGK45 induced a transient depletion of macrophages from the peripheral blood, with subsequent accumulation in the spleen (fig. S7, A and B). To test whether CD40 mAb initially engages CD40 on peripheral blood macrophages, which then migrate into tissues, we compared the biodistribution of FGK45 with that of RB6-8C5, a mAb used as a control and specific for Gr-1 expressed on granulocytes and immature myeloid cells in peripheral blood (fig. S7, C and D). Within 2 to

10 min after systemic administration of RB6-8C5, Gr-1<sup>+</sup> cells in the peripheral blood were found to be coated with antibody (fig. S8A). In contrast, FGK45 was not found on the cell surface of F4/80<sup>+</sup> macrophages in peripheral blood (fig. S8A) nor was FGK45 internalized after binding to CD40 (fig. S8B). Instead, at 10 min, FGK45 was observed bound to leukocytes residing within the spleen, lymph nodes, and pancreas of KPC mice (fig. S9A). Within the tumor microenvironment, FGK45 was found initially to localize to peripancreatic lymph nodes (Fig. 3, A and B) and not the tumor (Fig. 3, A and C), in contrast to RB6-8C5, which bound leukocytes in the tumor periphery as early as 10 min after treatment (Fig. 3D). At 18 hours, FGK45 was observed bound to F4/80+ macrophages infiltrating the tumor but not lymph nodes (Fig. 3, A, E, and F; and fig. S9, B and C). The binding of FGK45 to leukocytes within the tumor microenvironment was found to occur in clusters of cells rather than diffusely. We observed no change in the frequency of macrophages in the pancreas after FGK45 treatment (fig. S10). To determine whether FGK45 binds to macro-

60%

50%

40%

30%

20%

10%

phages before their infiltration of tumors, we treated KPC mice with clodronate-encapsulated liposomes (CELs) to deplete systemic macrophages (fig. S11A). Because liposomes are not capable of traversing vascular barriers produced by capillary walls, CELs do not diffuse into tissues (20) and, therefore, do not deplete macrophages within tumors (fig. S11, B to E). When KPC mice were treated with CELs, however, FGK45 labeling was no longer detectable in the tumors (Fig. 3, A and G), despite the continued presence of CD40<sup>+</sup> macrophages within the tumor. These findings support the hypothesis that FGK45 binds to macrophages before their migration into tumors.

Depending on their phenotype, macrophages can either promote or inhibit tumor progression (21, 22). In the absence of any treatment, we found that tumor-associated macrophages were activated and capable of secreting IL-10, TNF- $\alpha$ , and IL-6 but had reduced expression of MHC class II molecules compared with splenic macrophages from tumor-bearing KPC mice and normal littermates (fig. S12). After treatment with FGK45, macrophages in KPC tumors and spleens

Tumor +

KPC Mø (IgG2a)

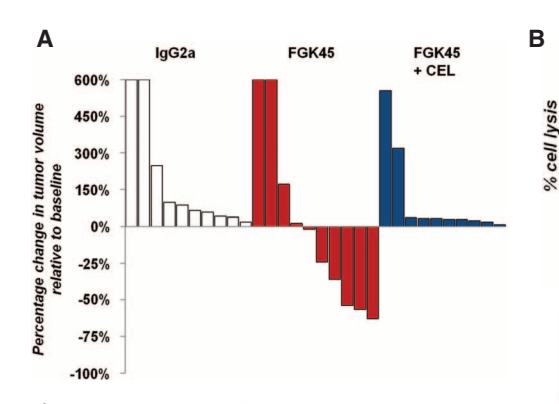
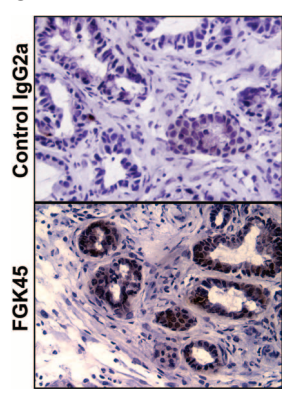
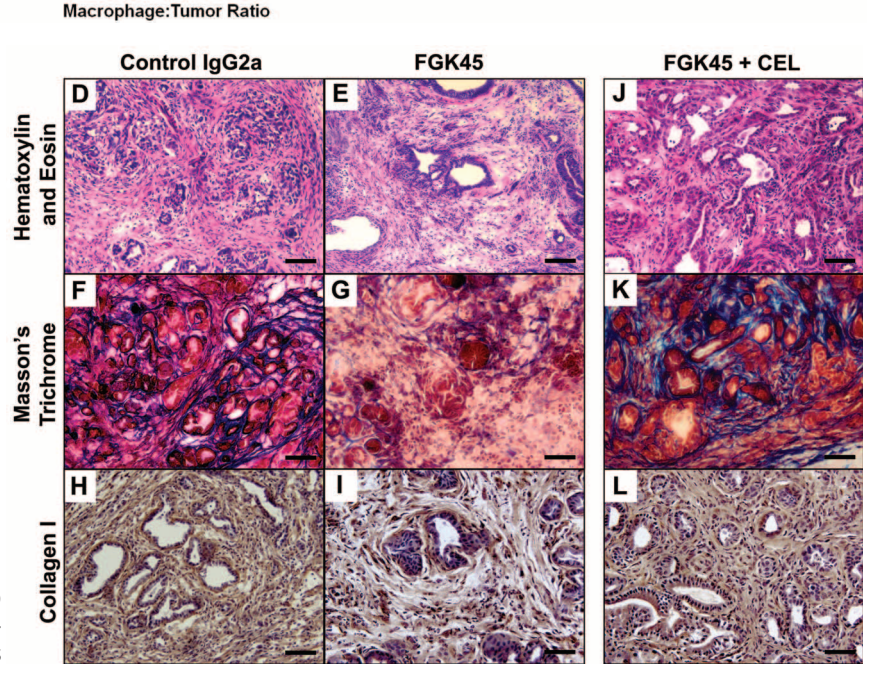


Fig. 4. CD40 activated tumor-infiltrating macrophages mediate tumor regression. (A) KPC mice were treated with control lgG2a or FGK45 or FGK45 plus depletion of systemic macrophages by means of CELs. Shown is a waterfall plot displaying percent change in tumor volume from baseline to day +14 (in comparison with IgG2a, FGK45: P < 0.05; FGK45 + CELs: P =1.00: Fisher's exact test).



(B) F4/80<sup>+</sup> tumor-associated macrophages were isolated from KPC mice that had been treated with FGK45 (blue squares) or control IgG2a (green circles) and incubated with KPC-derived tumor cell lines. Tumor cell death in vitro was measured by 7-aminoactinomycin D (7-AAD) labeling and

flow cytometric analysis at 24 hours. Shown is a representative assay from two independent experiments each performed in triplicate. Means  $\pm$  SD are depicted; \*P < 0.05, Student's t test. (C) Cleaved caspase 3 expression on KPC tumors was determined by immunohistochemistry 18 hours after treatment with control IqG2a (top panel) or FGK45 (bottom panel). (D) to (L)



7-AAD

10:1 30:1

KPC tumors were analyzed 18 hours after treatment with control IgG2a (**D**, **F**, and **H**), FGK45 (**E**, **G**, and **I**), or FGK45 + CEL (**J**, **K**, and **L**). Shown are hematoxylin-and-eosin histology (D, E, J); Masson's trichrome stain to reveal extracellular matrix in blue [(F), (G), and (K)], and immunohistochemistry for collagen I [(H), (I), and (L)]. Scale bars, 50 μm.

in tumor-bearing KPC mice up-regulated MHC class II and the costimulatory molecule CD86 with expression levels peaking at day 3 and returning to baseline after 7 days (Fig. 3H, and figs. S13 and S14). These changes coincided with a cytokine surge on day 1 after FGK45 treatment, with elevated serum levels of IL-12, TNF-α, and IFN-γ, but not IL-10, in KPC animals (fig. S15).

To determine whether macrophages were necessary for CD40-mediated tumor regression, we depleted systemic macrophages from KPC mice with CELs. Treatment with CELs abolished the capacity of FGK45 to induce tumor regression (Fig. 4A). Macrophages isolated from the pancreas of tumor-bearing KPC animals treated in vivo with FGK45 lysed tumor cells in vitro (Fig. 4B). This finding correlated with in vivo observations of cleaved caspase 3 expression in focal areas of the tumor at 18 hours after treatment with FGK45 (Fig. 4C). At this time after treatment, regions of the tumor stroma and associated fibrosis appeared to be undergoing involution (Fig. 4, D to G). These regions displayed a decrease in collagen I content, consistent with degradation of the tumor matrix (Fig. 4, H and I). In KPC mice depleted of systemic macrophages using CELs, FGK45 treatment failed to induce stromal degradation (Fig. 4, J to L). These findings identify a novel mechanism whereby the CD40 pathway can be harnessed therapeutically to restore tumor immune surveillance by targeting tumor-infiltrating macrophages involved in cancer inflammation.

PDA is a common, devastating, and highly lethal tumor for which new therapies are critically needed. Our findings identify a previously

unappreciated role for the CD40 pathway in regulating the immune reaction and fibrosis associated with PDA by reeducation of tumorassociated macrophages. Mechanistically, CD40 agonists altered tumor stroma and, in both mice and humans, showed efficacy against PDA. Although tumor-suppressing macrophages have been previously described (22), their role has been largely linked to the orchestration of T cell antitumor immunity. In this study, CD40 activation was, by itself, insufficient for invoking productive antitumor T cell immunity, and we hypothesize that full engagement of T cell immunity in PDA after CD40 activation will require modulation of additional tumor and host factors or the incorporation of novel vaccines (23). Our results emphasize that tumor immunosurveillance can at times be governed strictly by innate immunity under the regulation of the CD40 pathway and support the continued development of emerging therapeutic strategies that target inflammatory cells and stroma within the tumor microenvironment.

### **References and Notes**

- 1. H. A. Burris 3rd et al., I. Clin. Oncol. 15, 2403 (1997).
- 2. C. E. Clark et al., Cancer Res. 67, 9518 (2007).
- 3. S. P. Schoenberger, R. E. Toes, E. I. van der Voort, R. Offringa, C. J. Melief, Nature 393, 480 (1998).
- 4. S. R. Bennett et al., Nature 393, 478 (1998).
- 5. J. P. Ridge, F. Di Rosa, P. Matzinger, Nature 393, 474 (1998).
- 6. R. R. French, H. T. Chan, A. L. Tutt, M. J. Glennie, Nat. Med. 5, 548 (1999).
- 7. L. Diehl et al., Nat. Med. 5, 774 (1999).
- 8. E. M. Sotomayor et al., Nat. Med. 5, 780 (1999).
- 9. R. H. Vonderheide et al., J. Clin. Oncol. 25, 876

- 10. Materials and methods are available as supporting material on Science Online.
- 11. A. K. Nowak, B. W. Robinson, R. A. Lake, Cancer Res. 63, 4490 (2003).
- 12. R. A. Lake, B. W. Robinson, Nat. Rev. Cancer 5, 397 (2005).
- 13. D. I. Gabrilovich, Lancet Oncol. 8, 2 (2007).
- 14. L. Zitvogel et al., J. Clin. Invest. 118, 1991 (2008).
- 15. S. R. Hingorani et al., Cancer Cell 7, 469 (2005).
- 16. K. P. Olive et al., Science 324, 1457 (2009).
- 17. T. Van Dyke, Nat. Med. 16, 976 (2010).
- 18. R. H. Vonderheide, Clin. Cancer Res. 13, 1083 (2007).
- 19. C. van Kooten, J. Banchereau, J. Leukoc. Biol. 67, 2 (2000).
- 20. N. Van Rooijen, A. Sanders, J. Immunol. Methods 174,
- 21. L. M. Coussens, Z. Werb, Nature 420, 860 (2002).
- 22. A. Mantovani, A. Sica, Curr. Opin. Immunol. 22, 231
- 23. E. M. Jaffee et al., J. Clin. Oncol. 19, 145 (2001).
- 24. We thank C. Abrams, E. Furth, C. June, B. Keith, G. Koretzky, C. Simon, and B. Stanger for helpful discussions. This research was supported by the Abramson Family Cancer Research Institute of the University of Pennsylvania School of Medicine (R.H.V.) and by NIH grants P30 CA016520 (P.I.O. and R.H.V.) and K12 CA076931 (G.L.B.). The clinical study and part of the preclinical studies were supported by funding from Pfizer Corp (to R.H.V. and P.J.D). W. Song, D. Li, and L. L. Sharp are employees of Pfizer Corp. P. J. O'Dwyer discloses receiving honoraria from Pfizer; D. A. Torigian owns stock in Pfizer. CP-870,893 is owned and patented by Pfizer Corp., which manages its distribution. Although now at a new address, R. D. Huhn was affiliated with Pfizer Corp. during the conduct and analysis of this study. Some of the clinical data were presented at the 2010 American Society of Clinical Oncology Annual

### Supporting Online Material

www.sciencemag.org/cgi/content/full/331/6024/1612/DC1 Materials and Methods Figs. S1 to S15

References

29 September 2010; accepted 14 February 2011 10.1126/science.1198443

# **Cortical Constriction During Abscission Involves Helices** of ESCRT-III—Dependent Filaments

Julien Guizetti, 1,2 Lothar Schermelleh, 3 Jana Mäntler, 4 Sandra Maar, 1 Ina Poser, 4 Heinrich Leonhardt, Thomas Müller-Reichert, 5,2\* Daniel W. Gerlich 1,2\*

After partitioning of cytoplasmic contents by cleavage furrow ingression, animal cells remain connected by an intercellular bridge, which subsequently splits by abscission. Here, we examined intermediate stages of abscission in human cells by using live imaging, three-dimensional structured illumination microscopy, and electron tomography. We identified helices of 17-nanometer-diameter filaments, which narrowed the cortex of the intercellular bridge to a single stalk. The endosomal sorting complex required for transport (ESCRT)-III co-localized with constriction zones and was required for assembly of 17-nanometer-diameter filaments. Simultaneous spastin-mediated removal of underlying microtubules enabled full constriction at the abscission site. The identification of contractile filament helices at the intercellular bridge has broad implications for the understanding of cell division and of ESCRT-III-mediated fission of large membrane structures.

bscission represents the very final step of cell division in animal cells whereby the two daughter cells are physically severed from one another. The mechanism of abscission is poorly understood (1-3), but it may involve mechanical tearing (4) followed by

plasma membrane wound healing (5). An alternative model proposes that Golgi- (6) or recycling endosome (7)-derived vesicles establish membrane separation from within the intercellular bridge.

To clarify which events lead to abscission, we imaged live HeLa cells stably expressing enhanced green fluorescent protein (EGFP)-αtubulin (Fig. 1, A and B) (8). At the intercellular bridge, microtubule bundles gradually narrowed to a diameter of 0.97  $\pm$  0.13  $\mu$ m (mean  $\pm$  SD; n =17 cells) and then disassembled on one side

<sup>1</sup>Institute of Biochemistry, Department of Biology, Swiss Federal Institute of Technology Zurich (ETHZ), Schafmattstrasse 18, CH-8093 Zurich, Switzerland. <sup>2</sup>Marine Biological Laboratory (MBL), Woods Hole, MA 02543, USA. 3Department of Biology, Center for Integrated Protein Science Munich, Ludwig Maximilians University Munich, Grosshaderner Strasse 2, D-82152 Planegg-Martinsried, Germany. 4Max Planck Institute for Molecular Cell Biology and Genetics, Pfotenhauerstrasse 108, D-01307 Dresden, Germany. 5 Medical Theoretical Center, Medical Faculty Carl Gustav Carus, Dresden University of Technology, Fetscherstrasse 74, D-01307 Dresden, Germany.

\*To whom correspondence should be addressed. E-mail: daniel.gerlich@bc.biol.ethz.ch (D.W.G.); mueller-reichert@